NANO LETTERS

2009
Vol. 9, No. 5
2153-2159

Nanoparticle Superstructures Made by Polymerase Chain Reaction: Collective Interactions of Nanoparticles and a New Principle for Chiral Materials

Wei Chen,[†,‡] Ai Bian,[‡] Ashish Agarwal,[†] Liqiang Liu,[‡] Hebai Shen,[§] Libing Wang,[‡] Chuanlai Xu,[*,‡] and Nicholas A. Kotov[*,†,||]

Department of Chemical Engineering, University of Michigan, Ann Arbor, Michigan, 48109, School of Food Science and Technology, Jiangnan University, Wuxi, 214122, People's Republic of China, School of Life & Environment Science, Shanghai Normal University, Shanghai, 200234, People's Republic of China, and Departments of Materials Science and Biomedical Engineering, University of Michigan, Ann Arbor, Michigan, 48109

Received March 8, 2009

ABSTRACT

Polymerase chain reaction (PCR) was realized on the surface of gold nanoparticles (NPs) as a tool for self-organization at nanoscale and as a step toward programmable production of sufficient quantities of functional metallic superstructures. The assembly is controlled by varying the density of the primer on the surface of gold NPs and the number of PCR cycles generating a mixture of dimers, trimers, tetramers, etc., with gradually increasing complexity. This process leads to strong chirality of the assemblies arising from the three-dimensional positioning of NPs in space which had never been observed before. A circular dichroism band of the superstructures coincides with the plasmon oscillations of the multi-NP systems of Au colloids. This new collective optical property of NPs embracing the diversity of shapes and diameters in the starting dispersions opens unique opportunities for the development of negative index materials.

The construction of (metal) materials through self-assembly (SA) is an attractive alternative to lithography and traditional chemical synthesis of complex compounds. It requires, however, the extensive development of a synthetic toolbox making possible control over feature size and geometry of the assemblies in one-,[1−3] two-,[4−6] and three-dimensional systems.[7−14] Although many synthetic routes to nanoparticles (NPs), nanowires, nanoprisms, nanopyramids, and other nanocolloids with special shapes and compositions have been established, their controlled spatial arrangement remains a fascinating challenge in nanotechnology.[1−11] A variety of SA schemes have been developed on the basis of DNA, proteins, small organic molecules, and synthetic polymers as particle linkers.[1,3,15−17] Besides the ability to control interparticle distances,[18,19] NP periodicities,[10,11] and components of SA systems,[4,6,16] biological macromolecules have important advantage against the other structure-directing agents because (a) the geometry of the resulting assemblies can be very complex potentially competing with the organization of some cellular organelles, and (b) the synthesis of biological macromolecules is so well-developed that can potentially be computerized for the cases when NPs are also involved. The last point becomes very essential for making multi-NP systems available in sufficient quantities for research needs and applications.

Considering the utility of NP superstructures, we want to point out that besides the challenge of "how" one should assemble three-dimensional (3D) systems from NPs, there is also a major question of "what" needs to be assembled. *Au fond*, the functionality of the resulting assemblies, needs to originate from the collective properties of NPs rather than from the properties of individual components. In this respect, plasmonic interactions of metal NPs leading to the change of the dispersion color and enhancement of Raman scattering in the gaps between NPs for sensing application dominate the pool of background ideas at the moment.[1−18] Some attention was also given to the multiparticle superstructures for electronics involving charge transport phenomena at nanoscale.[8,20−22] In all these cases, however, the requirements

* Corresponding authors, xcl@jiangnan.edu.cn and kotov@umich.edu.
[†] Department of Chemical Engineering, University of Michigan.
[‡] School of Food Science and Technology, Jiangnan University.
[§] School of Life & Environment Science, Shanghai Normal University.
[||] Departments of Materials Science and Biomedical Engineering, University of Michigan.

10.1021/nl900726s CCC: $40.75
Published on Web 03/25/2009

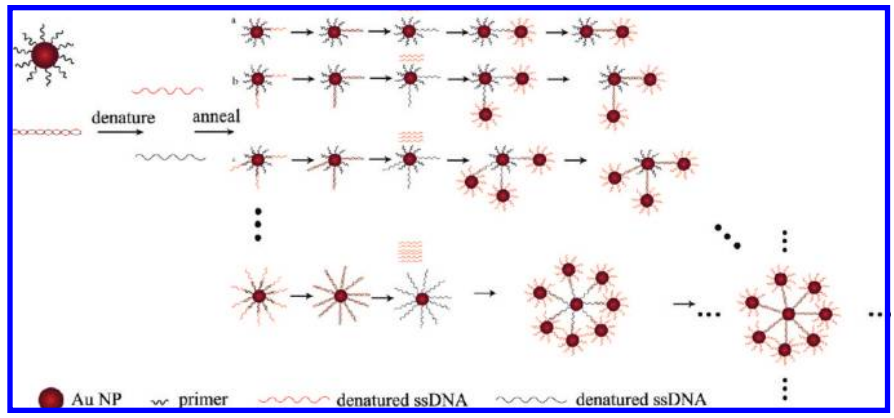

Figure 1. Schematics of SA through the PCR on Au NPs. The DNA polymerization process is analogous to traditional PCR and includes all the typical steps, such as denaturation, annealing, and extension.

to the 3D systems from the functional standpoint are fairly simple and, except for some cases of surface-enhanced Raman spectroscopy, the distance control is more important than the actual geometry of the superstructure.

Thus, in this study, we wanted to achieve the following goals: (1) to make a step toward realization of standard computerized assembly of the NPs; (2) to demonstrate a new type of 3D superstructure from NPs with a different principle behind their organization than those used previously, the *positioning* of NPs in space rather than the distance between them is the source of new properties of the multiparticle superstructures. Such systems can be exceptionally useful for negative index materials (NIMs)[23−25] as well as for sensors based on birefringence of optical media.

Among biomacromolecules, DNA−NP conjugates can be especially convenient for accomplishing these tasks because of extensive amount of structural information available for them. DNA−gold NP conjugates and their subsequent SA reactions have been studied extensively since 1996.[1,3] They are typically made by ligand exchange reaction between DNA carrying a thiol or amino moiety and citrate- or phosphine-coated gold NPs. The direct hybridization of the two single-stranded DNAs or their hybridization through a duplex bridge DNA are the two basic approaches of controlled attachment of one NP to another.[1−8,26] In order to achieve software control SA process, these methods need to be augmented by the polymerase chain reaction (PCR) on the surface of the gold NPs.

PCR is one of the most popular techniques in modern biological and medical sciences. It has revolutionized molecular genetics and other branches of biology/medicine. Owing to the exponential amplification of product in the enzyme-catalyzed DNA polymerization reaction, one could start from a single copy of target DNA and produce large amounts of it.[27−29] PCR is typically carried out in a liquid phase system, although recently it was extended to solid surfaces such as: nylon, glass, and microtiter well.[30] To date, the junction between PCR and nanocolloids was limited to the improvement of the efficiency/specificity of polymerization process by NPs and their use as probes for process completion.[31,32] While the technological feasibility of the PCR on the surface of NPs was recently demonstrated by some of us,[33] the use of PCR as a tool for controlled SA of NPs and, moreover, the new optical functionality of the resulting materials have not been demonstrated before and represents the primary scientific contents of this report.

Figure 1 illustrates the approach used here to the SA of NPs by PCR. The polymerization reaction takes place directly on the surface of Au NPs. The complexity of the SA material and the average number of nearest neighbors in it is controlled by the number of PCR cycles, N, and hence, by corresponding synthetic programs and PCR software. One should also expect that, the complexity of the formed SA materials is correlated with the density of the primers on the surface of Au NPs. We used here two densities of primer on Au NPs—low and high (Supporting Information). One can indeed see the some dependence of the resulting assemblies on this parameter, but no drastic changes in assembly patterns were observed, only the number of particles involved.

As expected, at early stages of the PCR, the structure of SA materials is comparatively simple (Figure 2A−C). Besides N, the number of particles in PCR products depends on the number of primers participated in the polymerization reactions. For high primer conditions, for $N = 1$, we see not only dimers, although they dominate, but also some amount of trimers as well. Panels M and N of Figure 2 are particularly representative of this point. In addition to monomers, SA aggregates with two, three, four, and five NPs are present in the mixture.

Under the condition of low primers on the Au NPs surface (Figure 2), SA structures after $N = 2$ are also predominantly dimers and monomers. When $N = 5$, trimers are the main products, when $N = 10$, there are both dimers and trimers and even tetramers in the products (Figure S1 in Supporting Information), and when $N = 40$, the complex agglomerates appear in the products similarly to the case with high primer coverage (Figure S1 in Supporting Information). Obviously the greater the number of primers coating NPs, the greater the number of NPs in the SA system, which conforms very well to expectations from PCR schematics (Figure 1). The selective preparation of a particular multimer (dimer, trimer, tetramer, etc.) can be obtained only after the stage of separation of different products. This is common for all

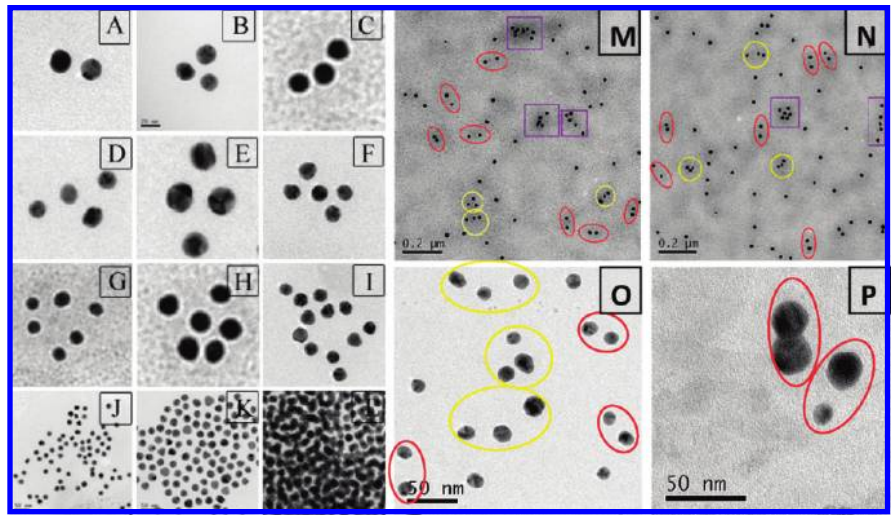

Figure 2. TEM images of PCR products. (A−L) Some characteristic SA aggregates of NPs observed after the number of PCR cycles indicated in the top left corner of the image with high primer concentration. (M, N) Representative TEM images describing the variety of SA products after five PCR cycles with high (exhaustive) concentration of the primer on Au NPs. (O, P) Representative TEM images describing the variety of SA products after five PCR cycles with low concentration of the primer on Au NPs. Approximately assigned dimers, trimers, and multimers are marked by red, yellow, and purple rectangles, respectively.

nanoparticle assemblies. Recently a new method of NP separation, field-flow electrophoresis (FFE), was established,[34] which can be particularly well applied to the separation of the NP multimers.

Note that assignment of the NPs to a specific multimer was done based on visual proximity of particles in transmission electron microscopy (TEM) images. We attempted a less subjective assignment of SA structures by using ImageJ (NIH) image processing software, but the algorithm for such an assignment has to include a step of arbitrary separation one aggregate from another. Also, there is always some amount of monomers that may accidently be in proximity of another aggregate, causing an error in assignment of the SA structure. This issue cannot be accounted for by the image processing software. It is an intrinsic problem of TEM images that cannot visualize DNA bridges between the NPs. Hence, we decided to present the actual TEM images, such as Figure 2M,N and Figure S1 (Supporting Information), rather than the misleading results of software processing. Although not without a degree of subjectivity, this way to assign NP assemblies to different multimer suits well for general description of the trend, which is important here, but it is probably not suitable for quantitative evaluation of the multimer distribution.

Regardless of this issue, the general tendency established by TEM imaging is quite clear: as the number of PCR cycles increases, the number of NPs in SA structures also increases. Two points need to be made regarding the structure of resulting assemblies. First, as expected, the reduction of the concentration of the primer on the surface of NPs reduces the average number of NPs in agglomerates (Figure 2O,P). As such, we can hardly assign any combination of NPs in Figure 2O to tetramers and pentamers for low concentration of the primer but there are a lot of dimers and trimers. Second, the size distribution of NPs in the dispersion used is relatively wide. There is also some variety of shapes of NPs when they noticeably deviate from the geometry of perfect spheres. Consequently, the SA structures after PCR are likely to contain NPs of different diameters and some variety of shapes. For the specific optical characteristics of the assemblies being considered below (Figure 5), this is not only a problem as for some other applications requiring NP monodispersity but also a desirable and necessary feature.

PCR products were further investigated by agarose gel electrophoresis (Figure 3). Overall, multimers with large numbers of particles are virtually completely retained at the start line. We did not observe bands attributable to specific multimer geometry for $N = 1-5$.[35] This is likely to be associated with a greater length of DNA used here than in previous studies. Well-formed bands were only observed for high $N > 10$ (Figure 3,E,F). TEM images indicate that the front band is primary formed by the monomers and potentially dimers (Figure 3G). The second band contains predominantly trimers and dimers (Figure 3H). Importantly, the electroporetic results clearly confirmed the trends identified after TEM examination (Figure 2): the increase of number PCR cycles results in the increase of the average number of NPs in the SA aggregate. The primer density was determined according the method from refs 36 and 37 to be 27.2 ± 1.4 and 108.8 ± 4.3 pmol/cm^2 for the limited and exhaustive primers, respectively. Similarly, the numbers of the primers on every single Au NP are about 29 and 153 for limited and exhaustive, respectively. The data for low (Figure 3 A,B,F) and high concentration of primer (Figure 3C,D,E) also coincide very well with TEM data (Figure 2O,P) indicating that a lower number of NPs is included in SA agglomerates when the density of primer on NPs is reduced. All together, the TEM and gel electrophoresis data are in agreement with expected results of PCR being carried out directly on the NP surface (Figure 1).

To further establish the nature of SA structures obtained after PCR and exclude the possibility of nonspecific ag-

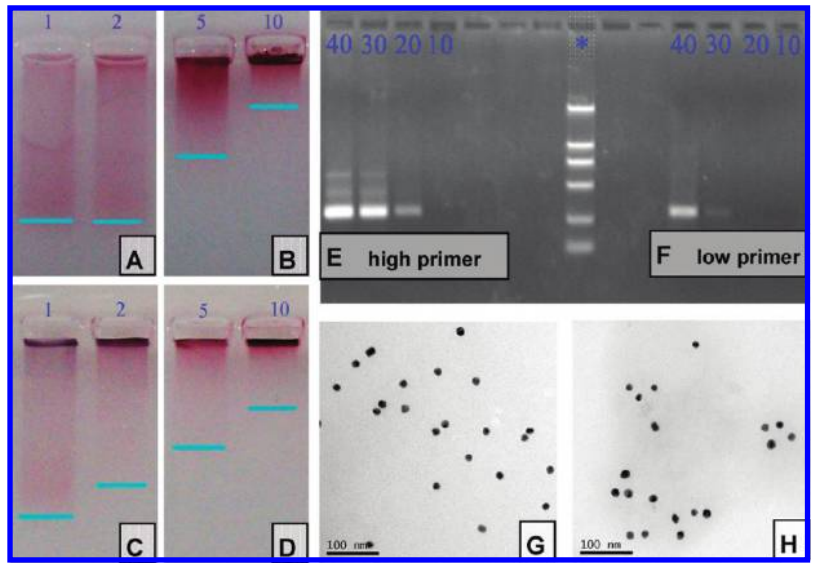

Figure 3. Gel electrophoresis data for SA products by PCR. (A−D) Optical images of gel electrophoretic plates for a low number of PCR cycles. (A, B) Low and (C, D) high concentrations of primers on the surface of Au NPs. The number of PCR cycles, *N*, is given on the top of the bands. The aquamarine line below denotes the position of the front. (E, F) Electrophoretic bands for a high number of PCR cycles for high (E) and low (F) concentrations of primers on the surface of Au NPs with EB stain. The number of PCR cycles, *N*, is given at the top of the bands. The center band marked (*) is the standard reference ladder. (G, H) TEM image of the recovered materials from the front band (G) and the second band (H) after electrophoretic separation in (E).

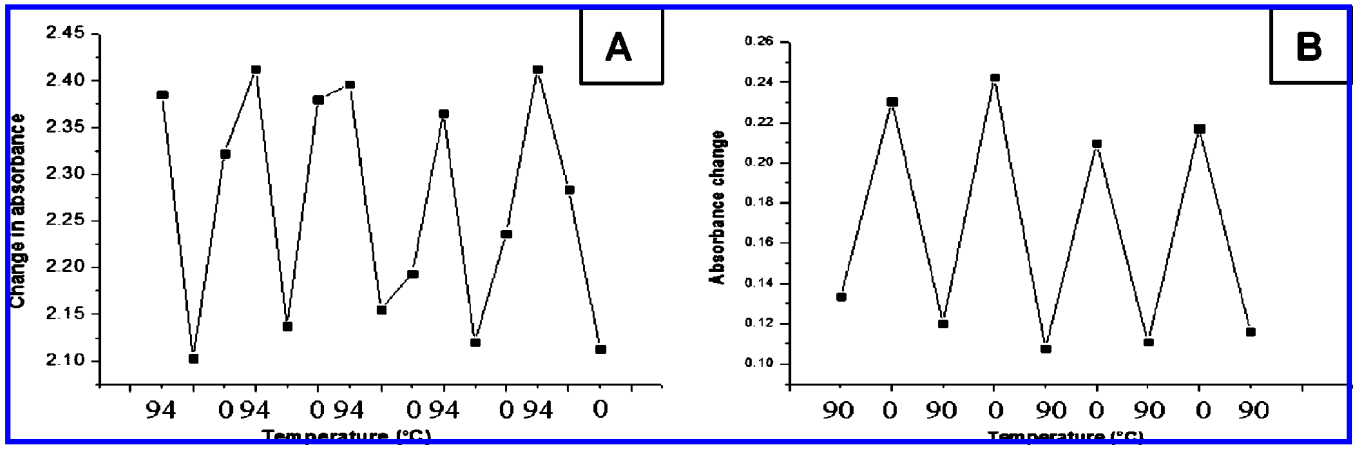

Figure 4. Absorbance change vs temperature/time profile for SA agglomerates after $N = 5$ for (A) 260 nm and (B) 700 nm.

glomeration of NPs without DNA hybridization, products after $N = 5$ were collected and resuspended in 1 M aqueous NaCl buffered at pH 7. The temperature/time dissociation experiment was performed by monitoring the optical absorption dependent on hybridization of DNA at 260 nm and on the degree of colloid aggregation at 700 nm due to coupling of plasmonic bands of individual NPs (Figure 4). As the temperature is cycled between 0 and $t = 94$ °C, which is 39 °C above the dissociation temperature (T_m) for the PCR-made DNA-duplex ($T_m = 55$ °C), we see the concomitant increase of adsorption at 260 nm and reduction of adsorption at 700 nm when $t = 90-94$ °C. The effect is reversed when $t = 0$ °C. The heating−cooling cycle can be repeated as many times as necessary (Figure 4), which indicates the reversibility of the SA phenomena and the fact that indeed the PCR products are made as a result of DNA hybridization.

Considering the relative rigidity of duplex DNA strands, the oligonucleotide bridges connecting the NPs together also determine (with a certain dynamic component) their preferred distribution in space. This property of the SA systems represents the primary area of interest for us in this work. As demonstrated in Figure 5A,B, the 3D structures of NP can be chiral when the particles are not identical to each other. They may vary by size (predominantly) as well as shape. In this case, the fact that the dispersions used here have a noticeable size distribution comes quite handy. Statistically, it is more probable than not that all the constituent NPs in the PCR-made superstructures, such as trimers, tetramers, or pentamers (Figure 2), shall be different. Consequently, such organization can give rise to ***chirality*** of NP assemblies manifesting in the circular dichroism (CD) signal. Some of the possible arrangements of NPs (Figure 5C) have strong resemblance with well-known chirality of organic molecules with four different ligands in tetrahedral spatial organization. Indeed, PCR products for $1 < N < 10$ reveal strong CD signals at 650 nm (Figure 5D), while none

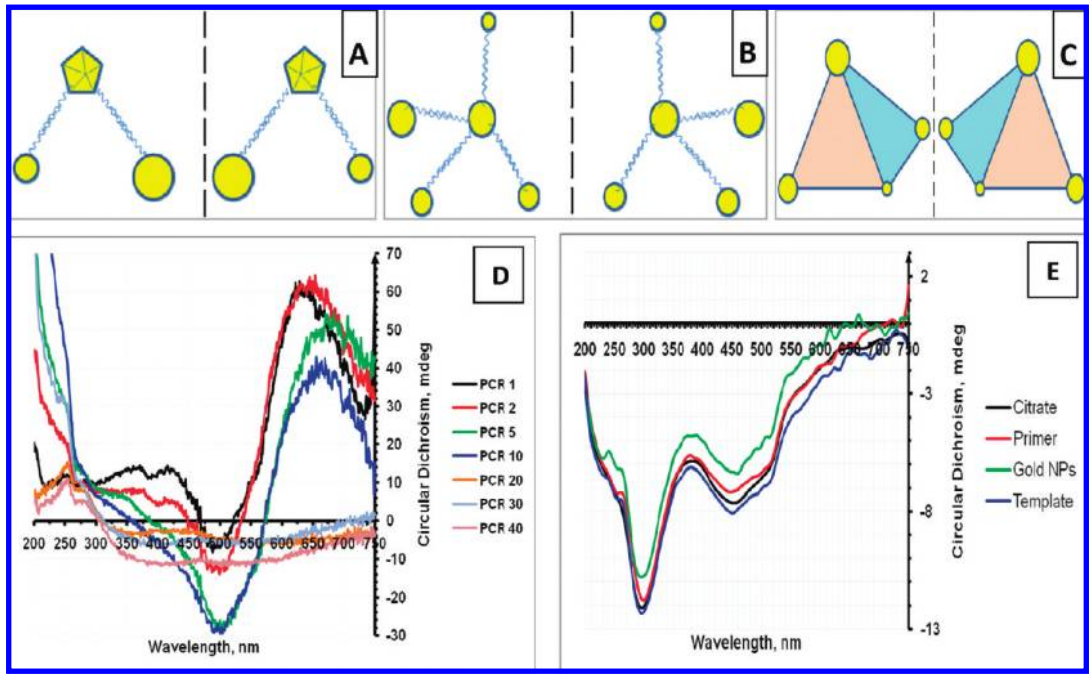

Figure 5. (A−C) Schematics of chiral NP superstructures. (D, E) Circular dichroism spectra of (D) products of PCR for increasing number of cycles, and (E) solutions of assembly components. Notice the difference in scales for vertical axes in (D) and (E).

of the components (Figure 5E) display any circular dichroism in this part of spectrum. In fact, the CD signal for the single NPs and solutions of other components in citrate buffer is determined largely by citrate. CD signal corresponding to DNA can be seen at 250−280 nm after subtraction of the signal for citrate (Figure S2 in Supporting Information). A fairly strong CD signal can be observed even for $N = 1$ when predominantly dimers and trimers are present. Besides existence of tetramers and pentamers in small quantities possible for $N = 1$, the appearance of chirality for such structures can be easily rationalized by taking into account the variety of shapes and sizes as described in Figure 5A, because the nonspherical particles of different diameters no longer have a plane of symmetry passing through them. In fact, even dimers from asymmetrical NPs can be chiral given significant 3D character of the assembly. As the number of PCR cycles increases and exceeds $N = 10$, very complex agglomerates are formed (Figure 2K,L) and CD signal disappears. Although many of the SA agglomerates produced by PCR satisfy the general schematics in Figure 5A−C, the large and fairly disorganized structures forming for big N values have approximately spherical or cylindrical symmetry and certainly possess no chirality. When the Au NPs have low density of primers, one could still observe some small CD signals at 650 nm (Figure S3 in Supporting Information) corresponding to the formation of some number of mutimers, such as trimers and tetramers. However, it is much lower compared to the case of a high density of primers especially for low N. This corresponds very well with the observation that there are, in general, a smaller number of particles in PCR products made on Au NP with a low density of primers (Figures 2 and 3). Note that statistically one would expect that the mixture of SA structures from NP as described in Figure 5A−C would be racemic; that is, no preference to the assemblies of particular chirality will be given. However, this is obviously not the case and there is a strong positive CD signal. The reasons behind the preference of a particular chirality in NP assemblies are currently unknown. One can speculate that the multimer mixture can be enriched by specific optical isomers due to the general preference of certain chirality in biological structure-directing agents.

Discussing the optical properties of SA structures, one significant aspect needs to be pointed out. The band where circular dichroism occurs correlates very well with the band of collective plasmonic resonances of Au NP assemblies. Moreover, the position of CD peak shifts to the red part of the spectrum as the number of PCR cycles and, hence, particles in the superstructure increases. The analogous red shift is typical for UV−vis adsorption spectra of NPs for increasing number of metal centers in the assemblies, which confirms the plasmonic nature of the CD band. This is a fundamentally different CD signal compared to that observed before in Au and other NPs.[38−41] Previously, the circular dichroism peak was attributed to the chiral defect sites on the surface of NPs caused by chiral stabilizers.[42−44] No observations have been made to date about chirality as a result of *collective* behavior of NPs. This is a new phenomenon for NP assemblies, which is dependent primarily on the 3D arrangement of NPs and to a lesser extent on the distance between them.

Finally, one should briefly address the utility of this optical property of SA assemblies. The practical aspects of the chiral SA systems can be understood considering the chiral effects on refractive index, n. According to the theory developed in refs 45–49, when n becomes smaller than the chirality parameter κ, the material may display negative index of refraction (NIM). There are no experimental observations yet of NIM properties stemming from chirality[45,46,48,50] due

to the lack of convenient experimental models and sufficient amounts of the material, which can be resolved by PCR on a NP surface. Although, there is no clear answer yet how n and κ for the described assemblies compare, the chiral properties of these structures and the position of the CD signal in the near-infrared region of the spectrum, which is very convenient for NIM devices, warrant further investigation in this area.

In conclusion, we have successfully prepared the SA materials by the PCR based on the solid interface of the NPs. The construction of the SA materials can be controlled by altering the parameters of the PCR program. The prepared SA materials possess novel optical properties resulting from the chiral spatial organization of NPs in SA superstructures. Better theoretical description of these optical properties based on calculations of ideal 3D structures similar to those presented in Figure 5A−C is much needed. Improvement of the separation methods of different oligomers will also be highly desirable for systematic studies of their chiral properties.

Acknowledgment. This research was supported by the MURI and GameChanger projects from AFOSR (N.A.K.) and National Natural Science Foundation of China 20871060 (C.X.). W. Chen and A. Bian fulfilled the experiments equally and cowrote the paper. A.A. analyzed the results and cowrote the paper. H. Shen, C. Xu, and N. Kotov conceived and designed the experiments and analyzed the results. L. Liu and L. Wang prepared the gold NPs and helped with apparatus construction and sample preparation.

Supporting Information Available: A description of the methods used and figures showing additional TEM images and circular dichroism spectra of components and products. This material is available free of charge via the Internet at http://pubs.acs.org.

References

(1) Alivisatos, A. P.; et al. Organization of 'nanocrystal molecules' using DNA. *Nature (London)* **1996**, *382*, 609–611.
(2) Deng, Z. X.; Tian, Y.; Lee, S. H.; Ribbe, A. E.; Mao, C. D. DNA-encoded self-assembly of gold nanoparticles into one-dimensional arrays. *Angew. Chem., Int. Ed.* **2005**, *44*, 3582–3585.
(3) Mirkin, C. A.; Letsinger, R. L.; Mucic, R. C.; Storhoff, J. J. A DNA-based method for rationally assembling nanoparticles into macroscopic materials. *Nature (London)* **1996**, *382*, 607–609.
(4) Liz-Marzan, L. M.; Mulvaney, P. The Assembly of Coated Nanocrystals. *J. Phys. Chem. B* **2003**, *107*, 7312–7326.
(5) Qin, W. J.; Yung, L. Y. L. Nanoparticle-DNA conjugates bearing a specific number of short DNA strands by enzymatic manipulation of nanoparticle-bound DNA. *Langmuir* **2005**, *21*, 11330–11334.
(6) Taton, T. A.; Mucic, R. C.; Mirkin, C. A.; Letsinger, R. L. The DNA-mediated formation of supramolecular mono- and multilayered nanoparticle structures. *J. Am. Chem. Soc.* **2000**, *122*, 6305–6306.
(7) Claridge, S. A.; et al. Directed assembly of discrete gold nanoparticle groupings using branched DNA scaffolds. *Chem. Mater.* **2005**, *17*, 1628–1635.
(8) Niemeyer, C. M. Progress in "engineering up" nanotechnology devices utilizing DNA as a construction material. *Appl. Phys. A: Mater. Sci. Process.* **1999**, *68*, 119–124.
(9) Niemeyer, C. M. Nanoparticles, proteins, and nucleic acids: Biotechnology meets materials science. *Angew. Chem., Int. Ed.* **2001**, *40*, 4128–4158.
(10) Nykypanchuk, D.; Maye, M. M.; van der Lelie, D.; Gang, O. DNA-guided crystallization of colloidal nanoparticles. *Nature (London)* **2008**, *451*, 549–552.
(11) Park, S. Y.; et al. DNA-programmable nanoparticle crystallization. *Nature (London)* **2008**, *451*, 553–556.
(12) Storhoff, J. J.; Mirkin, C. A. Programmed materials synthesis with DNA. *Chem. Rev.* **1999**, *99*, 1849–1862.
(13) Tao, A. R.; Habas, S.; Yang, P. D. Shape control of colloidal metal nanocrystals. *Small* **2008**, *4*, 310–325.
(14) Yin, Y. D.; Erdonmez, C. K.; Cabot, A.; Hughes, S.; Alivisatos, A. P. Colloidal synthesis of hollow cobalt sulfide nanocrystals. *Adv. Funct. Mater.* **2006**, *16*, 1389–1399.
(15) Brust, M.; Bethell, D.; Kiely, C. J.; Schiffrin, D. J. Self-assembled gold nanoparticle thin films with nonmetallic optical and electronic properties. *Langmuir* **1998**, *14*, 5425–5429.
(16) Cao, Y. W.; Jin, R.; Mirkin, C. A. DNA-modified core-shell Ag/Au nanoparticles. *J. Am. Chem. Soc.* **2001**, *123*, 7961–7962.
(17) Park, S. J.; Lazarides, A. A.; Mirkin, C. A.; Letsinger, R. L. Directed assembly of periodic materials from protein and oligonucleotide-modified nanoparticle building blocks. *Angew. Chem., Int. Ed.* **2001**, *40*, 2909–2912.
(18) Yao, H.; Kojima, H.; Sato, S.; Kimura, K. Interparticle spacing control in the superlattices of carboxylic acid-capped gold nanoparticles by hydrogen-bonding mediation. *Langmuir* **2004**, *20*, 10317–10323.
(19) Zhao, W. A.; Gao, Y.; Kandadai, S. A.; Brook, M. A.; Li, Y. F. DNA polymerization on gold nanoparticles through rolling circle amplification: Towards novel scaffolds for three-dimensional periodic nanoassemblies. *Angew. Chem., Int. Ed.* **2006**, *45*, 2409–2413.
(20) Claridge, S. A.; Liang, H. Y. W.; Basu, S. R.; Frechet, J. M. J.; Alivisatos, A. P. Isolation of discrete nanoparticle - DNA conjugates for plasmonic applications. *Nano Lett.* **2008**, *8*, 1202–1206.
(21) Katz, E.; Willner, I. Integrated nanoparticle-biomolecule hybrid systems: Synthesis, properties, and applications. *Angew. Chem., Int. Ed.* **2004**, *43*, 6042–6108.
(22) Cassagneau, T.; Mallouk, T. E.; Fendler, J. H. Layer-by-layer assembly of thin film zener diodes from conducting polymers and CdSe nanoparticles. *J. Am. Chem. Soc.* **1998**, *120*, 7848–7859.
(23) Shalaev, V. M.; et al. Negative index of refraction in optical metamaterials. *Opt. Lett.* **2005**, *30*, 3356–3358.
(24) Soukoulis, C. M.; Linden, S.; Wegener, M. Negative refractive index at optical wavelengths. *Science* **2007**, *315*, 47–49.
(25) Shalaev, V. M. Optical negative-index metamaterials. *Nat. Photonics* **2007**, *1*, 41–48.
(26) Portman, R. Design by DNA. *Nat. Nanotechnol.* **2008**, *3*, 132–132.
(27) Ding, C. M.; Cantor, C. R. A high-throughput gene expression analysis technique using competitive PCR and matrix-assisted laser desorption ionization time-of-flight MS. *Proc. Natl. Acad. Sci. U.S.A.* **2003**, *100*, 3059–3064.
(28) Lu, J. H.; et al. Positioning isolation and biochemical analysis of single DNA molecules based on nanomanipulation and single-molecule PCR. *J. Am. Chem. Soc.* **2004**, *126*, 11136–11137.
(29) Saiki, R. K.; et al. Primer-Directed Enzymatic Amplification of DNA with a Thermostable DNA-Polymerase. *Science* **1988**, *239*, 487–491.
(30) Turner, M. S.; et al. Solid-phase amplification for detection of C282Y and H63D hemochromatosis (HFE) gene mutations. *Clin. Chem.* **2001**, *47*, 1384–1389.
(31) Li, H. K.; et al. Nanoparticle PCR: Nanogold-assisted PCR with enhanced specificity. *Angew. Chem., Int. Ed.* **2005**, *44*, 5100–5103.
(32) Li, M.; Lin, Y. C.; Wu, C. C.; Liu, H. S. Enhancing the efficiency of a PCR using gold nanoparticles. *Nucleic Acids Res.* **2005**, *33*, e184.
(33) Shen, H. B.; Hu, M.; Wang, Y. B.; Zhou, H. Q. Polymerase chain reaction of nanoparticle-bound primers. *Biophys. Chem.* **2005**, *115*, 63–66.
(34) Ho, Szushen; Critchley, Kevin; Lilly, G. Daniel; Shim, Bongsup; Kotov, Nicholas A. Free flow electrophoresis for the separation of CdTe nanoparticles. *J. Mater. Chem.* **2009**, *19*, 1390–1394.
(35) Fu, A. H.; et al. Discrete nanostructures of quantum dots/Au with DNA. *J. Am. Chem. Soc.* **2004**, *126*, 10832–10833.
(36) Demers, M. L.; Mirkin, C. A.; Mucic, R. C.; Reynolds, R. A.; Letsinger, R. L.; Elghanian, R. A fluorescence-based method for determining the surface coverage and hybridization efficiency of thiol-capped oligonucleotides bound to gold thin films and nanoparticles. *Anal. Chem.* **2000**, *72*, 5535–5541.
(37) Jin, R. C.; Wu, G. S.; Li, Z.; Mirkin, C. A.; Schatz, G. C. What controls the melting properties of DNA linked gold nanoparitlce assemblies. *J. Am. Chem. Soc.* **2003**, *125*, 1643–1654.
(38) Gautier, C.; Burgi, T. Chiral inversion of gold nanoparticles. *J. Am. Chem. Soc.* **2008**, *130*, 7077–7084.
(39) Shemer, G.; et al. Chirality of silver nanoparticles synthesized on DNA. *J. Am. Chem. Soc.* **2006**, *128*, 11006–11007.

(40) Schaaff, T. G.; Whetten, R. L. Giant gold-glutathione cluster compounds: Intense optical activity in metal-based transitions. *J. Phys. Chem. B* **2000**, *104*, 2630–2641.
(41) Yao, H.; Miki, K.; Nishida, N.; Sasaki, A.; Kimura, K. Large optical activity of gold nanocluster enantiomers induced by a pair of optically active penicillamines. *J. Am. Chem. Soc.* **2005**, *127*, 15536–15543.
(42) Elliott, S. D.; Moloney, M. P.; Gun'ko, Y. K. Chiral shells and achiral cores in CdS quantum dots. *Nano Lett.* **2008**, *8*, 2452–2457.
(43) Li, T. H.; Park, H. G.; Lee, H. S.; Choi, S. H. Circular dichroism study of chiral biomolecules conjugated nanoparticles. *Nanotechnology* **2004**, *15*, S660−S663.
(44) Moloney, M. P.; Gun'ko, Y. K.; Kelly, J. M. Chiral highly luminescent CdS quantum dots. *Chem. Commun.* **2007**, 3900–3902.
(45) Cheng, Q.; Cui, T. J. Negative refractions in uniaxially anisotropic chiral media. *Phys. Rev. B* **2006**, *73*, -.
(46) Jin, Y.; He, S. L. Focusing by a slab of chiral medium. *Opt. Express* **2005**, *13*, 4974–4979.
(47) Mackay, T. G. Plane waves with negative phase velocity in isotropic chiral mediums. *Microwave Opt. Technol. Lett.* **2005**, *45*, 120–121.
(48) Pendry, J. B. A chiral route to negative refraction. *Science* **2004**, *306*, 1353–1355.
(49) Yannopapas, V. Negative index of refraction in artificial chiral materials. *J. Phys.: Condens. Matter* **2006**, *18*, 6883–6890.
(50) Baev, A.; Samoc, M.; Prasad, P. N.; Krykunov, M.; Autschbach, J. A quantum chemical approach to the design of chiral negative index materials. *Opt. Express* **2007**, *15*, 5730–5741.

NL900726S